Earth **Surface**
Dynamics
Discussions

1 **Pluri-decadal (1955–2014) evolution of glacier–rock glacier**

2 **transitional landforms in the central Andes of Chile**

3 **(30–33ºS)**

4

5 **S. Monnier[1], C. Kinnard[2]**

6 [1]{Instituto de Geografía, Pontificia Universidad Católica de Valparaíso, Valparaíso, Chile}

7 [2]{Département des Sciences de l'Environnement, Université du Québec à Trois-Rivières,

8 Trois-Rivières, Québec, Canada}

9 Correspondence to: S. Monnier (sebastien.monnier.ucv@gmail.com)

10

11 **Abstract**

12 This study deals with relationships between debris-covered glaciers and rock glaciers in the

13 central Andes of Chile. Three glacier–rock glacier transitional landforms are investigated over

14 the last decades in order to highlight and question the significance of their landscape

15 evolution and dynamics. We use series of historical air photos and Geoeye satellite images

16 together with common remote sensing operations including imagery orthorectification, digital

17 elevation model generation, and cross-correlation image matching. At each site, the following

18 items were monitored: rock glacier morphology, thermokarst area, horizontal surface

19 displacements and vertical surface displacements. The evolution of the landforms is

20 remarkable given the short time span of the study, with horizontal surface displacements up to

21 more than 3 m yr^{-1} and vertical displacements up to more than $\pm$ 1 m yr^{-1}. The landforms

22 studied reveal different evolutional significance: (i) overlap of glacier and rock glacier

23 development; (ii) glacier–rock glacier transformation; (iii) glacier–rock glacier collision.

24 Insights are gained for the second case: the transformation may take place by the division and

25 mixing of the buried ice body into distinct flow lobes and/or the apparent upward progression

26 of the rock glacier morphology by the successive incorporation of debris-covered glacier

27 patches.

28

1 **Key words:**

2 Rock glacier; Debris-covered glacier; Landscape evolution; Kinematics; Remote Sensing

3

4 **1 Introduction**

5 Glacier–rock glacier relationships have constituted a much investigated and debated issue in

6 high mountain studies over the last decades. These relationships are best expressed in large

7 glacier–rock glacier transitional landforms which are assemblages of debris-covered glaciers

8 in their upper part and rock glaciers in their lower part (e.g., Kääb et al., 1997; Krainer and

9 Mostler, 2000; Bodin et al., 2010; Janke et al., 2015). Rock glaciers are homo- or

10 heterogeneous ice–rock mixtures in permafrost state that move downslope by gravity-driven

11 creep. Debris-covered glaciers are glaciers covered with a thin and discontinuous debris

12 surface layer and which move by gravity-driven creep and sometimes basal slip in response to

13 a mass balance gradient, without the need for a permafrost state. Rock glaciers and debris-

14 covered glaciers exhibit distinct morphologies. Rock glacier morphology is coherent, stable,

15 and suggestive of viscous flow, with spatially organized features such as neat and steep

16 frontal and lateral margins, ridge-and-furrow patterns, and individual lobes. On the other

17 hand, debris-covered glacier morphology is chaotic and unstable, with unevenly distributed

18 features such as hummocks, crevasses, meandering furrows, and thermokarst.

19 According to the literature, at least three types of glacier–rock glacier relationships can be

20 distinguished:

21　(i)　The readvance and superimposition/embedding of a glacier or debris-covered

22　　　glacier onto/into a rock glacier, with related geomorphological and thermal

23　　　consequences (e.g., Lugon et al., 2004; Haeberli, 2005; Kääb and Kneisel, 2006;

24　　　Ribolini et al., 2007; Monnier et al., 2014). This is the *stricto sensu* significance of

25　　　'glacier–rock glacier relationships' (Haeberli, 2005) as defined by what has been

26　　　called the 'permafrost school' in reference to the long-term 'rock glacier

27　　　controversy' (see Berthling, 2011).

28　(ii)　The continuous derivation of a rock glacier from a pre-existing glacier, following

29　　　the progressive burial of the glacier by debris and further conservation and creep

30　　　of a massive and continuous core of glacier ice (e.g., Potter, 1972; Johnson, 1980;

31　　　Whalley and Martin, 1992; Potter et al., 1998; Humlum, 2000). This process was

Earth **Surface**
Dynamics
Discussions

Open Access

EGU

1   not initially called a 'glacier–rock glacier relationship'; this view is indeed held by

2   what has been called the 'continuum school' in opposition to the permafrost

3   school. Nevertheless, such phenomenon does belong, literarily, to the domain of

4   glacier–rock glacier relationships.

5   (iii)   The transformation of a debris-covered glacier into a rock glacier by the evolution

6   of the debris-covered ice body into a perennially frozen ice–rock mixture –

7   whatever the content and distribution of its internal ice. This has been described as

8   an alternative to the dichotomous debate between the permafrost school and

9   continuum school (Monnier and Kinnard, 2015); such phenomenon has been

10   described as achievable over human life or historical time scale (Schroder et al.,

11   2000; Monnier and Kinnard, 2015; Seppi et al., 2015).

12   In the present study, we aim to provide insights into the aforementioned issue using the

13   variety of glacier–rock glacier transitional landforms encountered in the semiarid Andes of

14   Chile and Argentina. These landforms have shown a particularly rapid evolution over the last

15   decades which allow studying glacier–rock glacier relationships on an historical time scale.

16   Three landforms with completely distinct morphologies have been chosen in the central

17   Andes of Chile in an attempt to diagnose the type of ongoing glacier–rock glacier

18   relationships and their geomorphological significance. To this purpose, this study makes use

19   of aerial and satellite imagery as well as remote sensing techniques in order to document the

20   dynamic evolution of the studied landforms over a pluri-decadal time span.

21   **2   Study sites**

22   We studied three glacier–rock glacier transitional landforms in the central Andes of Chile,

23   respectively named Navarro, Presenteseracae, and Las Tetas (Fig. 1). Navarro and

24   Presenteseracae are located in the Navarro valley, in the upper Aconcagua River catchment

25   (33º S). Las Tetas is located in the Colorado valley, in the upper Elqui River catchment (30º

26   S).

27   **2.1   Upper Navarro valley**

28   The upper Navarro valley belongs to the Juncal River catchment and Juncal Natural Park,

29   which are part of the upper Aconcagua River catchment, in the Valparaíso Region of Chile

30   (32°53' S, 70°02' W; Fig. 1). In the Juncal catchment (~1400–6110 m asl), glaciers cover

Earth **Surface**
Dynamics
Discussions

1   14% of the area (Bown et al., 2008; Ragettli et al., 2013) while active rock glaciers cover

2   almost 8% (Monnier and Kinnard, 2015). The climate is a mediterranean mountain climate.

3   Brenning (2005) and Azócar and Brenning (2010) located the 0°C isotherm of mean annual

4   air temperature (MAAT) close to 3700 m asl and defined precipitations above 3000 m asl as

5   ranging between 700 and 800 mm yr^{-1}. An automatic weather station located at 2800 m asl at

6   the foot of the Juncal glacier, 10 km SW from Navarro valley, recorded a MAAT of 6.3°C

7   during the hydrological year 2013−2014. The upper Navarro valley crosses, from west to east,

8   the Albánico formation (Upper Cretaceous; andesites, volcanic breccias), the San José

9   formation (Lower Cretaceous; limestones), and the Lagunilla formation (Upper Jurassic;

10   sandstones, lutites, gypsum). The glacial footprint is conspicuous through the Navarro valley:

11   the valley is U-shaped, with corries in the upper parts and latero-frontal moraines in the lower

12   parts (Fig. 2 and 3).

13   2.1.1 Navarro

14   Navarro fills the major part of the upper Navarro valley floor between ~3950 and 3450 m asl

15   (Fig. 3). The landform was described by Janke et al. (2015, p. 117) as a system composed of

16   several classes of debris-covered glaciers and rock glaciers according to their presumed ice

17   content. It is indeed a huge (>2 km long and up to >1 km wide) and complex assemblage with

18   debris-covered glacier morphology in its upper parts and a rock glacier morphology in its

19   lower parts. The main presumed flow direction of the landform points towards N170°. At least

20   ten conspicuous and sometimes >15 m high morainic crests are visible at the surface of the

21   landform, some of them being included in the rock glacier morphological unit. At one

22   location (red circle in Fig. 3), the superposition of two series of morainic crest onto a rock

23   glacier lobe suggests that the landform developed from a succession of glacier advances and

24   rock glacier development phases.

25   Navarro is divided between an eastern and a western unit; the two being separated by a central

26   series of aligned morainic crests (Fig. 3). The eastern unit, which is located in the north-

27   eastern part of Navarro valley, is ~1.2 km long, and about two thirds of its area exhibits a rock

28   glacier morphology. The terminal part exhibits three adjacent terminal lobes. The western unit

29   is ~2.4 km long and more complex. Sets of embedded morainic crests in the upper part

30   delimit the retreat of a former glacier. The median part (~1 km long) is peculiar, with the

31   boundary between the debris-covered and rock glacier morphology extending far downslope

32   and following the contour of an elongated central depression (10−15 m lower in altitude than

1 the lateral margins) (Fig. 3 and 4). This central depression is characterized by numerous and

2 large (up to 50 m of diameter) thermokarst depressions with bare ice exposures, generally on

3 their south-facing walls. The lower part of the western unit exhibits a rock glacier

4 morphology and three superimposed fronts close to the terminus, the slope of the lowest front

5 being gentler than that of the two upper fronts, which are almost at the same location.

6 Monnier and Kinnard (2015) provided an empirical model of permafrost probability based on

7 logistical regression for the upper Aconcagua River catchment. According to this model, the

8 upper parts of Navarro, especially the whole eastern unit, should be in permafrost conditions

9 (probability~1) (Fig. 3). On another hand, the model yielded a marked decreasing gradient in

10 permafrost probability from 0.9 to 0.7 between the central part and the terminus of the

11 western unit. It is worth noting that this decrease in permafrost probability correlates with the

12 thermokarst areas and central depression, the latter of which follows the pronounced

13 downslope inflection of the boundary between debris-covered and rock glacier morphology.

14 ## 2.1.2 Presenteseracae

15 Presenteseracae is a small (~600 m long and 300 m wide) debris-covered glacier located

16 between ~4080 and 3800 m asl, in a narrow, SW-facing cirque, ~300 m above and only 500

17 m east of Navarro (Fig. 3). The main presumed flow direction points towards N225º. This

18 landform has been thoroughly analysed by Monnier and Kinnard (2015). The debris-covered

19 glacier exhibits rock glacier features in its lower part (see also Fig. 4). The transverse and

20 curved ridges (<1.5 m high) and well-defined steep frontal talus slopes (~10 m high) have

21 appeared during the last 15 years. The permafrost model of Monnier and Kinnard (2015) gave

22 a permafrost probability of 1 for the whole Presenteseracae landform. The authors also

23 correlated the development of the coherent rock glacier morphology with the low estimated

24 sub-debris ice ablation rates, and demonstrated that the sediment store on Presenteseracae and

25 the potential formation times are in agreement with common rock wall retreat rates. They

26 concluded that Presenteseracae is a debris-covered glacier currently evolving into rock

27 glacier. In the upper part of the landform, the debris cover is very thin (a few cm) and bare ice

28 exposures are frequent. The debris cover thickens to more than 60 cm in the lower part, where

29 the rock glacier morphology develops below a steeper sloping segment. Small morainic crests

30 occur at the surface above 3780 m asl (Fig. 3). The lower part which displays a rock glacier

31 morphology is clearly composed of two adjacent lobes, dividing away from a morainic crest

32 overridden by the landform (Fig. 4). Depressed meandering furrows where buried ice is

1 exposed ice are also present. During hot summer days the water flowing in the northernmost

2 furrow sinks down a hole just before the front.

3 **2.2 Las Tetas**

4 Las Tetas is located in the Colorado valley, which is the uppermost part of the Elqui River

5 valley, in the Norte Chico Region of Chile (30°10' S, 69°55' W; Fig. 1). Elevations in the

6 Colorado valley range between ~3100 m asl and 6255 m asl. The landform is located on the

7 south-facing side of Cerro Las Tetas (5296 m asl), less than one km south of Glacier Tapado

8 (e.g., Ginot et al., 2006; Pourrier et al., 2014). The climate of the area is a semiarid mountain

9 climate. At the La Laguna artificial dam (~3100 m asl, 10 km west of the study site), the mean

10 annual precipitation was 167 mm during the 1970–2009 period, and the mean annual air

11 temperature was 8°C during the 1974–2011 period. The 0°C-isotherm is located near 4000 m

12 asl (Brenning, 2005; Ginot et al., 2006). Materials composing the rock basement belong to the

13 Pastos Blancos formation (Upper Palaeozoic; andesitic to rhyolitic volcanic rocks). A set of

14 embedded latero-frontal moraines is encountered ~700 m downslope from the front of Las

15 Tetas, between ~4170 and 4060 m asl.

16 Las Tetas is a ~1 km long landform located between 4675 and 4365 m asl (Fig. 5). The main

17 presumed flow direction points towards N140º. The boundary between debris-covered and

18 rock glacier morphology is clear and divides the landform in two approximately equal units.

19 The upper unit is characterized by a chaotic morphology, vast (up to more than 50 m of

20 diameter) and deep (up to 20 m) thermokarst depressions exposing bare ice generally along

21 their south-facing walls. The lower part of the landform exhibits tension cracks superimposed

22 onto the ridge-and-furrow pattern. The front of Las Tetas is prominent, almost 100 m high

23 (Fig. 4). According to the logistic regression-based empirical permafrost model proposed by

24 Azócar (2013) for the area, the 0.75 probability level crosses the landform in its central part

25 (Fig. 5).

26 **3 Material and methods**

27 **3.1 Satellite image and air photo processing**

28 We searched for and acquired historical air photos and more recent satellite images for the

29 three study sites. Stereo pairs of air photos were inspected, selected, and scanned at the

1 Geographic and Military Institute (IGM) of Chile. Scanning was configured in order to yield a

2 ground resolution of 1 m. At Las Tetas, photos from 1956, 1978, and 2000 were selected; at

3 Navarro and Presenteseracae (Navarro valley), photos from 1955 and 2000 were selected. A

4 stereo pair of Geoeye satellite images was also acquired for each site. The Geoeye stereo pairs

5 were acquired on 23 March 2012 and 14 February 2014 at Las Tetas and Navarro valley,

6 respectively, as panchromatic image stereo pairs (0.5 m of resolution) along with four bands

7 in the near-infrared, red, green, and blue spectra (2 m of resolution).

8 Orthoimages, orthophotos, and altimetric information were generated from the data. The first

9 step involved building a digital elevation model (DEM) from the stereo pair of Geoeye

10 satellite images. The Geoeye images were triangulated using a Rational Polynomial Camera

11 (RPC) model supplied by the data provider. The exterior orientation was constrained using

12 one or two ground control points (GCPs) acquired with a differential GPS system in the field

13 in 2014 over bedrock outcrops visible on the images. Sets of three-dimensional (3D) points

14 were extracted automatically using standard procedures of digital photogrammetry (Kääb,

15 2005) and edited manually to remove blunders. A 2×2 m DEM was generated using

16 triangular irregular network (TIN) interpolation of the 3D points. The same processing

17 scheme was used for the air photo stereo pairs. The vertical bias of the air photo DEMs was

18 calculated by comparison with the Geoeye DEMs over flat and stable areas outside the

19 landform studied and was removed from the subsequent calculations (see below). The

20 automatic and manual extraction of 3D points from air photo stereo pairs proved to be

21 challenging in steep areas with unfavourable viewing geometry. The process failed for the

22 1955 stereo pair of Navarro valley, with only a very sparse set of 3D points extracted and

23 including possible blunders, ruling out the possibility to generate a reliable and complete

24 DEM and estimate a vertical bias.

25 The Geoeye images were pansharpened and orthorectified using the Geoeye DEM. The air

26 photos were then orthorectified using the same Geoeye DEM; the orthorectification was

27 constrained by the internal camera information, tie points, and ground control points (GCPs)

28 extracted during the process. The accuracy of the orthorectification was estimated using the

29 GCPs. The root mean square error (RMSE) corresponding to the sets of GCPs at the different

30 times is displayed in Table 1. The ground resolution of the orthophotos was then resampled at

31 0.5 m in order to equal that of the Geoeye products.

1 The altimetric information was used to calculate the vertical displacement of the landforms

2 between the different dates (after removal of the vertical bias). The total vertical displacement

3 was further converted in annual rates of vertical displacement. As outlined by Lambiel and

4 Delaloye (2004), vertical displacements at the surface of rock glaciers may be explained by

5 several and possibly concomitant factors: downslope movement of the landform and

6 advection of local topographic features, extensive or compressive flow, and melting or

7 aggradation of internal ice. Therefore, it is difficult to unambiguously interpret vertical

8 changes. Studying the Muragl rock glacier (Swiss Alps), Kääb and Vollmer (2000)

9 highlighted how mass advection caused subtle vertical displacements (between -0.20 and

10 $+0.20$ m yr^{-1}), while surface lowering of up to -0.5 m yr^{-1} were considered as indicative of

11 massive losses of ice. Accordingly, taking into account the range of values measured and the

12 uncertainty (or detection threshold) on the measurements (see Table 2), we used an absolute

13 value of 0.50 m yr^{-1} to generally discriminate between 'moderate' and 'large' vertical

14 changes. The former were considered to relate primarily to the downslope expansion of the

15 landform; in the case of the latter, additional ice melting or material compression and bulging

16 were considered necessary in the interpretation.

17 **3.2 Image interpretation**

18 The geomorphology of each landform was carefully interpreted from the orthoimages and

19 orthophotos. The first aim was to locate, for each date, the boundary between the debris-

20 covered and rock glacier morphology. The thermokarst area was monitored over time by

21 mapping the thermokarst depressions at the surface of the landforms as polygonal shapes, and

22 their total area was calculated. Salient features such as curved ridges on Presenteseracae and

23 cracks on Las Tetas were also mapped.

24 **3.3 Image feature tracking**

25 We used a cross-correlation image matching technique in order to measure horizontal

26 displacements at the surface of the landforms. Cross-correlation image matching is a sub-

27 pixel precision photogrammetric technique that has been widely used for studying the

28 kinematics of glaciers, rock glaciers, and other mass movements. We followed the principles

29 and guidelines provided by Kääb and Vollmer (2000), Kääb (2005), Wangensteen et al.

30 (2006), Debella-Gilo and Kääb (2011), and Heid and Kääb (2012). The image correlation

1   software CIAS (Kääb and Vollmer, 2000; Heid and Kääb, 2012) was used for this purpose.

2   CIAS uses two orthoimages (from spaceborne, airborne, or terrestrial sensors) of the same

3   area and resolution taken from the same position but at different times. CIAS computes the

4   normalized cross-correlation (NCC) as an estimate of the similarity of image intensity values

5   between matching entities in the orthoimage at time 1 (I_1) and their corresponding entities in

6   the orthoimage at time 2 (I_2). In I_1, a 'search template' is defined around each pixel located

7   manually or automatically inside a regular grid; the software extracts this search template

8   from I_1 and search for it in I_2 within the area of a predefined search window (see Fig. 2 in

9   Debella-Gilo and Kääb, 2011, p. 132); the algorithm then computes the NCC coefficient

10   between the search template in I_1 and the one in I_2 and moves the search template until the

11   entire search window is covered. The location that yields the highest correlation coefficient

12   within the search window is considered as the likely best match for the original location in I_1.

13   The size of the search template and search window is defined by the operator. Once

14   measurements are achieved, results are filtered (Wangensteen et al., 2006).

15   For all sites we used a search template of 15 pixels, which fits the textural characteristics of

16   the surfaces. The search window size was defined depending upon the maximum expected

17   displacements (Kääb and Vollmer, 2000). The base of the front of the landform was digitized

18   when it was clearly identifiable on the orthoimages. Then for each time interval the maximum

19   front displacement was measured and used for defining the search window size accordingly

20   (Table 3). The precision of the measurement of the maximum front displacement was

21   estimated to be ±5 m taking into account the errors related both to orthorectification and the

22   mapping error on the images. Although the front displacements cannot be considered as

23   reflecting the displacements over the whole surface, they provide a good indicative lower

24   threshold of the values expected. Before measuring displacements on the landforms the

25   images were co-registered to one another a using polynomial transformation by matching

26   reference stable boulders (>1 m of diameter) or prominent rock outcrop corners between I_1

27   and I_2; the operation had to yield a RMSE less than or around 1 m in both x and y directions

28   before being validated. The NCC algorithm was performed over the whole area of the

29   landforms using a 5 m-spacing grid, except in the case of the 2000–2014 period at Navarro

30   where a 10 m-spacing grid was used in order to avoid too large an amount of data. The final

31   filtering procedure excluded points that did not meet the following three conditions: (i) the

32   displacement magnitude must be higher than the RMSE generated by the orthorectification

33   and co-registration steps (Table 2); (ii) the azimuthal deviation from the general landform

1   flow direction must be less than 50º; (iii) the cross-correlation coefficient must be higher than

2   0.5. The filtering step led to keep ~30% of the initial amount of points. Finally, the total

3   displacements measured by the program were converted in annual displacement rates, and the

4   displacement vectors were mapped and used to interpret the surface dynamics of the

5   landforms studied.

6   **4   Results**

7   **4.1   Navarro**

8   4.1.1 Rock glacier morphology

9   Rock glacier morphology areas have evolved spatially between 1955 and 2014, especially in

10 the eastern unit, where they now represent ~75% of the total area; the boundary between the

11 debris-covered and rock glacier morphologies has progressed upward considerably (~400 m)

12 between 1955 and 2014 (Fig. 6 and 7). In the western unit, the spatial progression of the rock

13 glacier morphology has been more limited and occurred inward from the margins; the lower

14 position of the boundary between debris-covered and rock glacier morphology has followed

15 the overall displacement of the feature and has not progressed upward.

16 4.1.2 Thermokarst area

17 Between 1955 and 2000, thermokarst area expanded from 11,950 to 16,520 m^2, before

18 shrinking by a factor of two in less than 15 years (8,560 m^2 in 2014). As thermokarst occurs

19 mainly in the central part of the western unit, this reduction has to be related to the

20 progression of the coherent morphology from the margins of the feature inward (see previous

21 subsection).

22 4.1.3 Horizontal surface displacements

23 Between 1955 and 2000, horizontal displacements at the surface of the Navarro landform

24 ranged between 0.09 and 0.91 m yr^{-1} and averaged 0.41 m yr^{-1} (Fig. 6). Between 2000 and

25 2014, horizontal displacements ranged between 0.06 and 0.96 m yr^{-1} and averaged 0.47 m

26 yr^{-1} (Fig. 7). On the whole, surface displacements of Navarro are constant from one period to

27 another. Also, the computed displacement rates are typical of rock glaciers (see, e.g., Barsch,

28 1996; Haeberli et al., 2006). Displacement rates reach their maximum behind the upper fronts

1 of the western unit and in the upper part of the three terminal lobes of the eastern unit, where

2 a break of slope occurs.

3 Displacement vector patterns are clearer over the 2000−2014 period (Fig. 7). This may be

4 explained by the quality of the images at the times considered and the related performance of

5 the feature tracking algorithm. This may also relate with the expansion of the rock glacier

6 morphology. One striking feature in Fig. 7 is indeed how displacement vector patterns are

7 more organized and expressive of coherent flow in rock glacier morphology areas than in

8 debris-covered glacier morphology areas where it is more chaotic. Moreover, from the upper

9 to the lower part of the landform and around the central depression of the western unit the

10 displacement vectors progressively rotate clockwise, first pointing mostly southward and then

11 increasingly towards the south-southwest. This is suggestive of a compressive flow regime,

12 and occurs also more locally in the terminus areas or along the lateral margins.

4.1.4 Vertical surface displacements

14 Vertical displacements of the surface between 2000 and 2014 are more pronounced in debris-

15 covered glacier morphology areas than in rock glacier morphology areas and in the western

16 unit than in the eastern unit (Fig. 7). Rock glacier areas exhibit overall moderate surface

17 lowering and local (fronts and margins) surface heaving; as precised in the Methods section,

18 the former must be related to the downslope expansion of the landform, and the latter to

19 material compression and bulging. Debris-covered glacier areas exhibit more contrasting

20 displacements. Large surface lowering has occurred particularly in the uppermost part, and in

21 the central part of the western unit. The lowering is largest along the central depression,

22 where it is seen as expressing the concomitance of extensive flow and downwasting owing to

23 ice losses. Significant local surface heaving has also occurred, such as in the upper part of the

24 western unit, owing to material compression and bulging.

4.2 Presenteseracae

4.2.1 Rock glacier morphology

27 The rock glacier morphology at the surface of Presenteseracae has appeared during the last 15

28 years (Fig. 8, 9 and 10). The fast evolution of the landscape was described by Monnier and

29 Kinnard (2015). Nowadays, the whole lower half of the landform exhibits rock glacier

30 morphology (Fig. 3, 4 and 10). In the southern part of the landform, however, this

1   morphology is less coherent; it is conspicuously cut by a central furrow and exhibits few areas

2   of bare ice over which debris slumps may occur. In the northern part of the landform, the rock

3   glacier morphology is more developed; there is neither remaining bare ice area nor evidences

4   of debris cover instability and sliding.

5   4.2.2 Thermokarst areas

6   No thermokarst areas have been identified at the surface of the landform during the studied

7   period.

8   4.2.3 Horizontal surface displacements

9   Between 1955 and 2000, horizontal displacements at the surface of the Presenteseracae

10   landform ranged between 0.14 and 3.47 m yr^{-1} and averaged 1.88 m yr^{-1} (Fig. 9). Between

11   2000 and 2014 period, horizontal displacements ranged between 0.08 and 2.28 m yr^{-1} and

12   averaged 1.22 m yr^{-1} (Fig. 10). Hence there is a slight decrease in velocity between

13   1955−2000 and 2000−2014. Displacements are one order of magnitude higher than those on

14   the surface of Navarro and appear as relatively high for rock glaciers. Their amplitude

15   correlates with the very fast landscape evolution at the site (Monnier and Kinnard, 2015).

16   Whereas displacement rates do not show any striking spatial variation, the analysis of the

17   displacement vector orientations together with the morphology highlight two flow lobes in the

18   upper part and two flow lobes in the lower part.

19   4.2.4 Vertical surface displacements

20   Between 2000 and 2014, the spatial pattern of vertical surface displacements follows the

21   boundary between the debris-covered and rock glacier morphologies in 2014 (Fig. 10). The

22   upper debris-covered glacier part is mainly affected by overall moderate surface lowering

23   owing to the downslope expansion of the landform, and localized (in the lower part) large

24   surface heaving owing to material compression and bulging. The lower rock glacier part

25   exhibits overall moderate surface lowering owing to downslope expansion, localized large

26   surface lowering owing to additional ice melting, and pronounced surface heaving along the

27   front of the landform, owing to pronounced material compression and bulging.

Earth **Surface**
Dynamics
Discussions

1   **4.3 Las Tetas**

2   4.3.1 Rock glacier morphology

3   The boundary between debris-covered and rock glacier morphology has only followed the

4   overall displacement of the landform (Fig. 11−13). There has not been any upward or lateral

5   progression of the rock glacier morphology. The main morphological evolution is the recent

6   apparition (between 2000 and 2012) of tension cracks in the lower part of the landform (Fig. 5

7   and 13).

8   4.3.2 Thermokarst area

9   Between 1956 and 1978, thermokarst areas remained quite stable (from 21,700 to 23,200 m^2).

10   The limits of thermokarst areas could not be identified clearly on the 2000 orthophoto. In

11   2012, the thermokarst area has decreased by a factor of two (11,100 m^2).

12   4.3.3 Horizontal surface displacements

13   Between 1956 and 1978, horizontal displacements at the surface of the Las Tetas landform

14   ranged between 0.15 and 1.48 m yr^{-1} and averaged 0.79 m yr^{-1} (Fig. 11). Between 1978 and

15   2000 period, horizontal displacements ranged between 0.24 and 1.98 m yr^{-1} and averaged

16   1.08 m yr^{-1} (Fig. 12). Finally, between 2000 and 2012, they ranged between 0.21 and 2.51 m

17   yr^{-1} and averaged 1.34 m yr^{-1} (Fig. 13). On the whole, the order of magnitude of the

18   horizontal displacements at the surface of Las Tetas is slightly lower than that measured at the

19   surface of Presenteseracae. There has been a clear increase in displacement speeds: between

20   1956 and 2012, the mean value has almost increased by a factor of two. Displacement rates do

21   not show any striking spatial variations; however, the analysis of the displacement vector

22   orientations on either side of the boundary between debris-covered and rock glacier

23   morphology reveals that these two areas may represent two distinct flow units, especially

24   since 1978. On the whole the displacement vector orientations and successive rates highlight

25   the landform longitudinal extension. Displacement vectors converge at the location of

26   thermokarst ponds, which indicates the collapse of thermokarst features (see below).

27   4.3.4 Vertical surface displacements

28   As in the Navarro case, there is an opposition between the upper debris-covered glacier area

29   and the lower rock glacier area (Fig. 11−13); nevertheless, note that between 2000 and 2012

Earth **Surface**
Dynamics
Discussions

1 (Fig. 13) most of the displacement rates are below the detection threshold (Table 2). In the

2 upper part, the general tendency is for moderate surface lowering owing to the downslope

3 expansion of the landform, with localized large surface lowering or heaving owing to the

4 evolution of thermokarst areas. The latter involves topographic feature displacement, ice

5 melting, and possible superficial mass movements of debris sliding over glacier ice. In the

6 lower part, moderate surface lowering generally predominates owing to the downslope

7 expansion of the landform; however, pronounced surface heaving has occurred locally owing

8 to material compression and bulging. Between 1956 and 2012, there has also been a

9 progressive decrease in vertical displacement rates. This decrease correlates, in the upper part,

10 with the decrease in thermokarst areas, which highlights a tendency towards a stabilization of

11 the surface morphology.

5   Interpretations and discussion

13 Each of the cases studied represents a specific type of glacier–rock glacier relationship which

14 reflects different landscape evolution trajectories.

5.1   Navarro: spatiotemporal overlap of glacier and rock glacier developments, and glacier–rock glacier transformation

17 Navarro is a debris-covered glacier–rock glacier assemblage which has resulted, as far as we

18 can look into the past, from the embedding of two debris-covered glaciers (a western one and

19 an eastern one) into pre-existing rock glaciers in the lower part of the landform. Between

20 2000 and 2014 (Fig. 7), this is reflected by the general compressive flow exhibited in the

21 lower part and the concomitant ice melt-driven downwasting of the central area at the

22 boundary between the debris-covered and rock glacier morphologies. These morphological

23 changes have resulted from the sustained displacement of a downwasting debris-covered

24 glacier into/onto a pre-existing rock glacier and lateral debris ridges. The boundary between

25 the debris-covered and rock glacier morphologies in 1955 (Fig. 6) gives a minimum

26 indication of the lowest advance of the debris-covered glaciers onto the rock glaciers.

27 The landform has evolved differently between the western and eastern unit. In the eastern

28 unit, the assemblage is turning into a single rock glacier; the rock glacier progressively

29 incorporates segments of the upper debris-covered glacier. Indeed: (i) from 1955–2000 to

30 2000–2014 (Fig. 6 and 7) the area of rock glacier morphology has expanded upward and now

Earth **Surface**
Dynamics
Discussions

1 covers ~75% of the eastern unit, and the displacement vectors describe a more generally

2 coherent, expansive flow; (ii) the moderate surface lowering between 2000 and 2014 can be

3 explained referring to the simple downslope extension of the landform (without additional ice

4 melt-driven downwasting); (iii) this presumed stability of the ice stock must be related to a

5 modelled permafrost probability close to 1. The situation is markedly different in the western

6 unit: there the debris-covered glacier–rock glacier assemblage is not turning into a single rock

7 glacier. (i) The limited progression of the rock glacier morphology between 1955 and 2014

8 correlates with an area of decreasing permafrost probability and marked ice melt-driven

9 downwasting along the centreline (Fig. 6 and 7). These conditions are little favourable for the

10 development of a coherent and stable rock glacier morphology. (ii) Displacement vectors,

11 especially between 2000 and 2014 (Fig. 7), separate the landform into three longitudinal units

12 with distinct though potentially interacting flow dynamics. In the upper part, a debris-covered

13 glacier lobe with little coherent flow is downwasting and advancing. In the central part, the

14 debris-covered glacier is advancing into lateral debris ridges and a rock glacier. Downslope,

15 the latter composes the lower unit. The rock glacier exhibits more coherent flow and is still

16 expanding, albeit moderately, at the expense of the debris-covered glacier, notably by 'eating'

17 away thermokarst areas. However, the morphological and dynamic boundaries throughout the

18 landform are very prominent: the rock glacier occurs as a rather isolated unit in an area with

19 unfavourable topoclimatic conditions, and the sustainment of its activity in the future is

20 questionable. The decreasing gradient in permafrost probability can also explain the subdued

21 activity of the lowest rock glacier lobe. This lobe is interpreted as compressed and maintained

22 active only by the backward push exerted by the upper lobe.

23 **5.2   Presenteseracae: glacier–rock glacier transformation**

24 The results brought in this study confirm and strengthen the conclusions reached by Monnier

25 and Kinnard (2015). Presenteseracae is a debris-covered glacier that has evolved into a rock

26 glacier during the last decades, with fast horizontal displacements and the apparition of a rock

27 glacier morphology in the lower part. The speed of displacement is currently slowing

28 (compare Fig. 8 and 9), which may reflect an acceleration of the transition towards a rock

29 glacier. Furthermore, the presence of distinct flow lobes throughout the landform shows that

30 this case of glacier-deriving rock glacier does not fit the common model of the glacier ice-

31 cored rock glacier where the evolution of the landform is controlled by the extension and

32 creep of a massive and continuous core of glacier ice (e.g., Potter, 1972; Whalley and Martin,

Earth **Surface**
Dynamics
Discussions

1   1992; Potter et al., 1998). Instead, Presenteseracae suggests that the internal glacier ice is

2   fragmenting into several bodies with distinct flow dynamics; this may be regarded as a

3   transition between a structure made of continuous buried glacier ice to one that mixes patches

4   of buried glacier ice, pore ice, segregated and intrusive ice, and debris entrained from the

5   surface.

6   5.3   Las Tetas: a simple case of a glacier colliding into a rock glacier

7   Las Tetas is a debris-covered glacier–rock glacier assemblage which has been most probably

8   and simply created from the readvance of a (debris-covered) glacier into the back of a rock

9   glacier. The debris-covered glacier and rock glacier have move together, which is seen in the

10 displacement vector patterns (Fig. 11–13), but their interaction remains limited: there is no

11 sign of an upward progression of the rock glacier morphology and no dynamic indication of a

12 superimposition/embedding of the debris-cover glacier onto/into the rock glacier. Due to the

13 rather even distribution of surface displacements, and in the absence of information on the

14 internal structure, it is impossible to assess if one of the two components of the landform is

15 leading the movement.

16 Despite the still chaotic and unstable morphology of the upper debris-covered glacier, the

17 decrease in thermokarst area, along with the occurrence of compression at the exact location

18 of the main thermokarst features and the progressive decrease of vertical displacement rates

19 over the entire period (Fig. 11–13), suggest an evolution towards a more stable flowing

20 morphology. Will the latter be a 'full' rock glacier? A presage may be how the upper part of

21 the landform is progressively 'eating' away the thermokarst. On another hand, the lower rock

22 glacier area developed a network of tension cracks during the last 15 years, while the whole

23 landform accelerated; it is also located in an area of lower permafrost probability. It is known

24 that the climate in the area is warming: Rabatel et al. (2011) reported a warming trend of

25 0.19ºC decade^{-1} for the 1958–2007 period in the Pascua-Lama area, 80 km north of Las

26 Tetas. Monnier et al. (2014) also reported a trend of 0.17ºC decade^{-1} for the 1974–2011

27 period in the Río Colorado area. Thus, Las Tetas is reminiscent of cases of destabilizing and

28 accelerating rock glaciers in response to air and permafrost temperature increases (Roer et al.,

29 2005 and 2008; Delaloye et al., 2010; Kellerer-Pirklbauer and Kaufmann, 2012) and the

30 permanence of the activity and the surface stability of the rock glacier in the future are

31 questionable.

6   Conclusion

We have used remote sensing techniques in order to highlight the evolution, on a human life-time scale, of three glacier−rock glacier transitional landforms in the central Andes of Chile. A noticeable landscape evolution was observed at the three studied sites, but the modalities and significance vary from one case to another:

(i)   Navarro is a complex landform resulting from successive glacier (re)advance and rock glacier development phases. While the eastern unit of the landform exhibits a progressive incorporation of the upper debris-covered glacier into the lower rock glacier, the western unit is more characterized by glacier ice melt-driven downwasting and limited rock glacier development. This difference is related to topoclimatic and permafrost conditions. The frequency of glacier advances through Navarro valley, reflected in well-preserved morainic features, suggests that by essence Navarro is a transitory landform.

(ii)   Presenteseracae is a special case of debris-covered glacier that has evolved into a rock glacier during the last decades, with the rock glacier morphology having mostly developed ~15 years ago. Horizontal surface displacements have been fast (up to more than 3 m yr^{-1}). The analysis of the displacement vector orientations has highlighted the development of distinct flow lobes.

(iii)   Las Tetas is a simple longitudinal assemblage between debris-covered and rock glacier. The landform moves as a whole, and the interactions between the debris-covered and rock glacier areas appear limited in comparison with the two other cases. The landform has accelerated over the studied period, which is reflected in the apparition of destabilization features (tension cracks) and a decrease in permafrost probability in the lower part of the landform, along with the ongoing climate warming trend in the area.

Our study helps to understand how different processes that shape mountain landscapes can overlap and relay each other both in time and space. We have also provided new insights into the glacier−rock glacier transformation problem. Most of the common and previous glacier−rock glacier evolution models depicted a 'continuum' process based on the preservation of an extensive core of buried glacier ice. On the contrary, our findings rather suggest that the transformation of a debris-covered glacier into a rock glacier may proceed from the upward progression of the rock glacier morphology at the expense of the debris-

17

1   covered glacier and/or the fragmenting of the debris-covered glacier into several ice–rock

2   mixture flow lobes. Regarding topoclimatic conditions and permafrost probabilities, the

3   evolution of the landforms studied here finally provide a strong support for the importance of

4   including the permafrost criterion in the rock glacier definition.

5

6   **Acknowledgements**

13

14 **References**

15 Azócar, G.F.: Modelling of permafrost distribution in the semiarid Chilean Andes. Master

16 Thesis, University of Waterloo, Canada, 2013.

17 Azócar, G.F., and Brenning, A.: Hydrological and geomorphological significance of rock

18 glaciers in the dry Andes, Chile (27°–33°S). Permafrost and Periglacial Processes, 21, 42–53,

19 2010.

20 Barsch, D.: Rockglaciers. Indicators for the present and former geoecology in high mountain

21 environments. Springer, Berlin, 1996.

22 Berthling, I.: Beyond confusion: rock glaciers as cryo-conditioned landforms.

23 Geomorphology, 131, 98–106, 2011.

24 Bodin, X., Brenning, A., Rojas, F.: Status and evolution of the cryosphere in the Andes of

25 Santiago (Chile, 33.5° S.). Geomorphology, 118, 453–464, 2010.

26 Bown, F., Rivera, A., and Acuña, C.: Recent glacier variations at the Aconcagua basin,

27 central Chilean Andes. Annals of Glaciology, 48, 43–48, 2008.

1   Brenning, A.: Climatic and geomorphological controls of rock glaciers in the Andes of central

2   Chile: combining statistical modelling and field mapping. Ph.D. Thesis, Humboldt University,

3   Berlin, 2005.

4   Davis, J.C.: Statistics and data analysis in geology. John Wiley & Sons, New York, 2002.

5   Debella-Gilo, M., Kääb, A.: Sub-pixel precision image matching for measuring surface

6   displacements on mass movements using normalized cross-correlation. Remote Sensing of

7   Environment, 115, 130−142, 2011.

8   Delaloye, R., Lambiel, C., Gärtner-Roer, I.: Overview of rock glacier kinematics research in

9   the Swiss Alps. Season rhythm, interannual variations and trends over several decades.

10 Geographica Helvetica, 65, 135−145, 2010.

11 Ginot, P., Kull, C., Schotterer, U., Schikowski, M., and Gäggeler, H.W.: Glacier mass balance

12 reconstruction by sublimation induced enrichment of chemical species on Cerro Tapado.

13 Climate of the Past, 2, 21–30, 2006.

14 Haeberli, W.: Investigating glacier−permafrost relationships in high-mountain areas:

15 historical background, selected examples and research needs. In: Harris, C., Harris, J.B.

16 (Eds.), Cryospheric systems: glaciers and permafrost. The Geological Society, London,

17 29−38, 2005.

18 Haeberli, W., Hallet, B., Arenson, L., Elconin, R., Humlum, O., Kääb, A., Kauffmann, V.,

19 Ladanyi, B., Matsuoka, M., Springman, S., Vonder Mühll, D.: Permafrost creep and rock

20 glacier dynamics. Permafrost and Periglacial Processes, 17, 189−214, 2006.

21 Heid T., Kääb A.: Evaluation of existing image matching methods for deriving glacier surface

22 displacements globally from optical satellite imagery. Remote Sensing of Environment, 118,

23 339−355, 2012.

24 Humlum, O.: The geomorphic significance of rock glaciers: estimates of rock glacier debris

25 volumes and headwall recession rates in West Greenland. Geomorphology 35, 41–67, 2000.

26 Janke, J.R., Bellisario, A.C., and Ferrando, F.A.: Classification of debris-covered glaciers and

27 rock glaciers in the Andes of central Chile. Geomorphology, 241, 98−121, 2015.

28 Johnson, P.G.: Glacier–rock glacier transition in the Southwest Yukon territory, Canada.

29 Arctic and Alpine Research, 12, 195–204, 1980.

1 Kääb, A.: Remote sensing of mountain glaciers and permafrost. Zürich University,
2 Switzerland, 2005.

3 Kääb, A., Kneisel, C.: Permafrost creep within a recently deglaciated forefield: Muragl, Swiss
4 Alps. Permafrost and Periglacial Processes, 17, 79−85, 2006.

5 Kääb, A., Vollmer, M.: Surface geometry, thickness changes and flow fields on creeping
6 mountain permafrost: Automatic extraction by digital image analysis. Permafrost and
7 Periglacial Processes, 11, 315−326, 2000.

8 Kääb, A., Haeberli, W., Gudmundsson, G.H.: Analysing the creep of mountain permafrost
9 using high precision aerial photogrammetry: 25 years of monitoring Gruben rock glacier,
10 Swiss Alps. Permafrost and Periglacial Processes, 8, 409−426, 1997.

11 Kellerer-Pirklbauer, A., Kaufmann, V.: About the relationships between rock glacier velocity
12 and climate parameters in Central Austria. Austrian Journal of Earth Sciences, 105, 94−112,
13 2012.

14 Krainer, K., Mostler, W.: Reichenkar rock glacier: a glacier-derived debris-ice system in the
15 western Stubai Alps, Austria. Permafrost and Periglacial Processes, 11, 267−275, 2000.

16 Lambiel, C., Delaloye, R.: Contribution of real-time kinematic GPS in the study of creeping
17 mountain permafrost: examples from the Western Swiss Alps. Permafrost and Periglacial
18 Processes, 15, 229−241, 2004.

19 Lugon, R., Delaloye, R., Serrano, E., Reynard, E., Lambiel, C., González-Trueba, J.J.:
20 Permafrost and Little Ice Age glacier relationships, Posets Massif, Central Pyrenees, Spain.
21 Permafrost and Periglacial Processes, 15, 207−220, 2004.

22 Monnier, S., and Kinnard, C.: Reconsidering the glacier to rock glacier transformation
23 problem: new insights from the central Andes of Chile. Geomorphology, 238, 47−55, 2015.

24 Monnier, S., Kinnard, C., Surazakov, A., Bossy, W.: Geomorphology, internal structure, and
25 successive development of a glacier foreland in the semiarid Andes (Cerro Tapado, upper
26 Elqui Valley, 30º08′ S., 69º55′ W.). Geomorphology, 207, 126−140, 2014.

27 Potter, N.: Ice-cored rock glacier, Galena Creek, Northern Absaroka Mountains,Wyoming.
28 Geological Society of America Bulletin, 83, 3025−3058, 1972.

1   Potter, N., Steig, E.J., Clark, D.H., Speece, M.A., Clark, G.M., Updike, A.U.. Galena Creek

2   rock glacier revisited — new observations on an old controversy. Geografiska Annaler, 80A,

3   251–265, 1998.

4   Pourrier, J. Jourde, H., Kinnard, C., Gascoin, S., and Monnier, S.: Glacier meltwater flow

5   paths and storage in a geomorphologically complex glacial foreland: the case of the Tapado

6   glacier, dry Andes of Chile (30° S.). Journal of Hydrology, 519A, 1068–1083, 2014.

7   Rabatel, A., Castebrunet, H., Favier, V., Nicholson, L., Kinnard, C. Glacie changes in the

8   Pascua-Lama region, Chilean Andes (29º S): recent mass balance and 50 yr surface area

9   variations. The Cryosphere, 5, 1029−1041, 2011.

10 Ragettli, S., Cortés, G., McPhee, J., Pellicciotti, F.: An evaluation of approaches for

11 modelling hydrological processes in high-elevation, glacierized Andean watersheds.

12 Hydrological Processes, 28, 5774−5695, 2012.

13 Ribolini, A., Chelli, A., Guglielmin, M., Pappalardo, M.: Relationships between glacier and

14 rock glacier in the Maritime Alps, Schiantala valley, Italy. Quaternary Research, 68, 353−363,

15 2007.

16 Roer, I., Kääb, A., Dikau, R.: Rockglacier acceleration in the Turtmann valley (Swiss Alps):

17 probable controls. Norsk Geografisk Tiddsskrift (Norwegian Journal of Geography), 59,

18 157−163, 2005.

19 Roer, I., Haeberli, W., Avian, M., Kaufmann, V., Delaloye, R., Lambiel, C., Kääb, A.:

20 Observations and considerations on destabilizing active rockglaciers in the European Alps. In:

21 Kane, D.L., Hinkel, K.M. (Eds.), Proceedings of the Ninth International Conference on

22 Permafrost, University of Alaska, Fairbanks, 1505−1510, 2008.

23 Schroder, J.F., Bishop, M.P., Copland, L., Sloan, V.F.: Debris-covered glaciers and rock

24 glaciers in the Nanga Parbat Himalaya, Pakistan. Geografiska Annaler, 82A, 17–31, 2000.

25 Seppi, R., Zanozer, T., Carton, A., Bondesan, A., Francese, R., Carturan, L., Zumiani, M.,

26 Giorgi, M., Ninfo, A.: Current transition from glacial to periglacial processes in the Dolomites

27 (South-Eastern Alps). Geomorphology, 228, 71−86, 2015.

28 Wangensteen, B., Guðmundsson, Eiken, T., Kääb, A., Farbrot, H., Etzelmüller, B.: Surface

29 displacements and surface age estimates for creeping slope landforms in Northern and Eastern

30 Iceland using digital photogrammetry. Geomorphology, 80, 59−79, 2006.

1   Whalley, W.B., Martin, H.E.: Rock glaciers. II. Models and mechanisms. Progress in Physical

2   Geography, 16, 127–186, 1992.

Table 1.

Errors generated during the air photo processing. The ground root mean square error (RMSE) relates to sets of ground control points (GCPs) extracted from the Geoeye orthoimage and used for the orthorectification of the air photos.

Site	Date	Horizontal ground RMSE (m)		Number of GCPs
		x	y	
Las Tetas	1956	0.92	0.93	5
	1978	1.13	1.16	10
	2000	0.33	0.54	8
Navarro valley	1955	1.82	1.32	13
	2000	0.76	1.49	9

Table 2.

Uncertainty related to the measurement of annual rates of vertical and horizontal displacements according to the period considered. The horizontal uncertainty takes into account both the ground RMSE related to the orthorectification (Table 1) and the RMSE related to the co-registration step in the cross-correlation image matching. The vertical uncertainty corresponds to the probability level associated with the standard deviation (σ) of the vertical bias of the generated DEMs. In Navarro valley, no reliable DEM could be generated from the 1955 air photos, which explains the absence of data in the table for the 1955−2000 interval.

Site	Period	Horizontal uncertainty (m yr^{-1})	Vertical uncertainty (m yr^{-1})	
			1σ (66%)	2σ (95%)
Las Tetas	1956−1978	0.17	0.11	0.21
	1978−2000	0.15	0.04	0.09
	2000−2012	0.11	0.22	0.43
Navarro valley	1955−2000	0.10	—	—
	2000−2014	0.15	0.05	0.10

Earth **Surface**
Dynamics
Discussions

1   **Table 3.**

2   Use of the maximum front displacement measured on orthophotos between times for defining the size
3   of the search window involved in the CIAS algorithm. Further, the longest displacement computed by
4   the program can be compared with the maximum front displacement, giving an indication of the
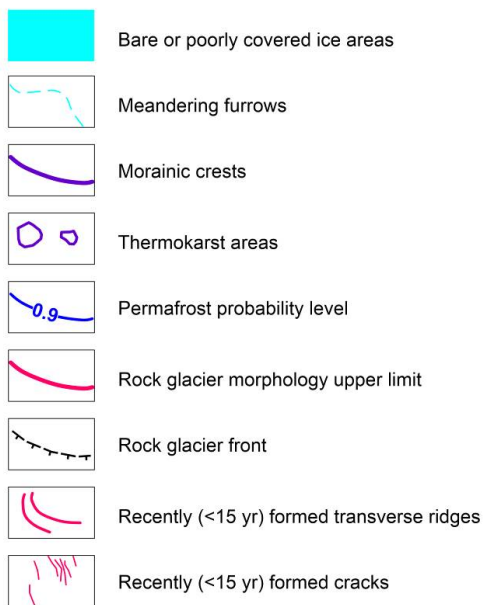5   method reliability.

6

Landform	Time interval	Maximum front displacement measured		Selected search window (pixels)	Longest displacement computed (m)
		metres	pixels		
Navarro	1955–2000	30	60	150	41
	2000–2014	<5	≥10	50	13
Presenteseracae	1955–2000	120	240	500	156
	2000–2014	25	50	100	32
Las Tetas	1956–1978	20	40	100	32
	1978–2000	15	30	80	23
	2000–2012	20	40	100	30

7

1
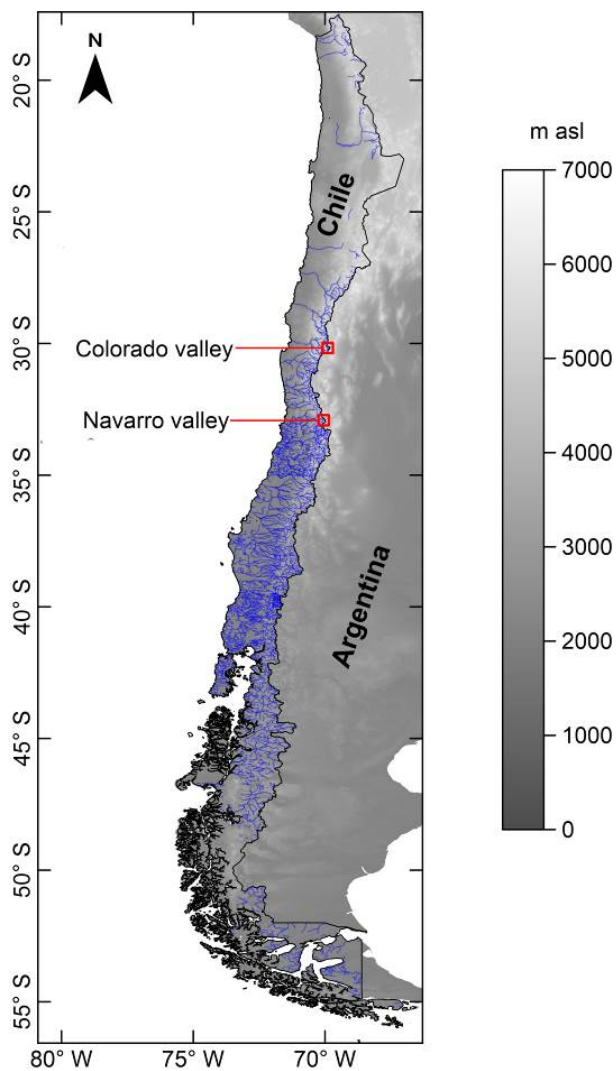
Figure 1. Location of the study sites. Drainage network is shown in blue.

▮ (cyan)	Bare or poorly covered ice areas
⌇	Meandering furrows
⌒	Morainic crests
⬡ ⬭	Thermokarst areas
0.9	Permafrost probability level
⌒	Rock glacier morphology upper limit
⌒⌒⌒	Rock glacier front
⌒⌒	Recently (<15 yr) formed transverse ridges
⋔	Recently (<15 yr) formed cracks

1

2   **Figure 2.** Geomorphological legend shared for all subsequent figures.

1
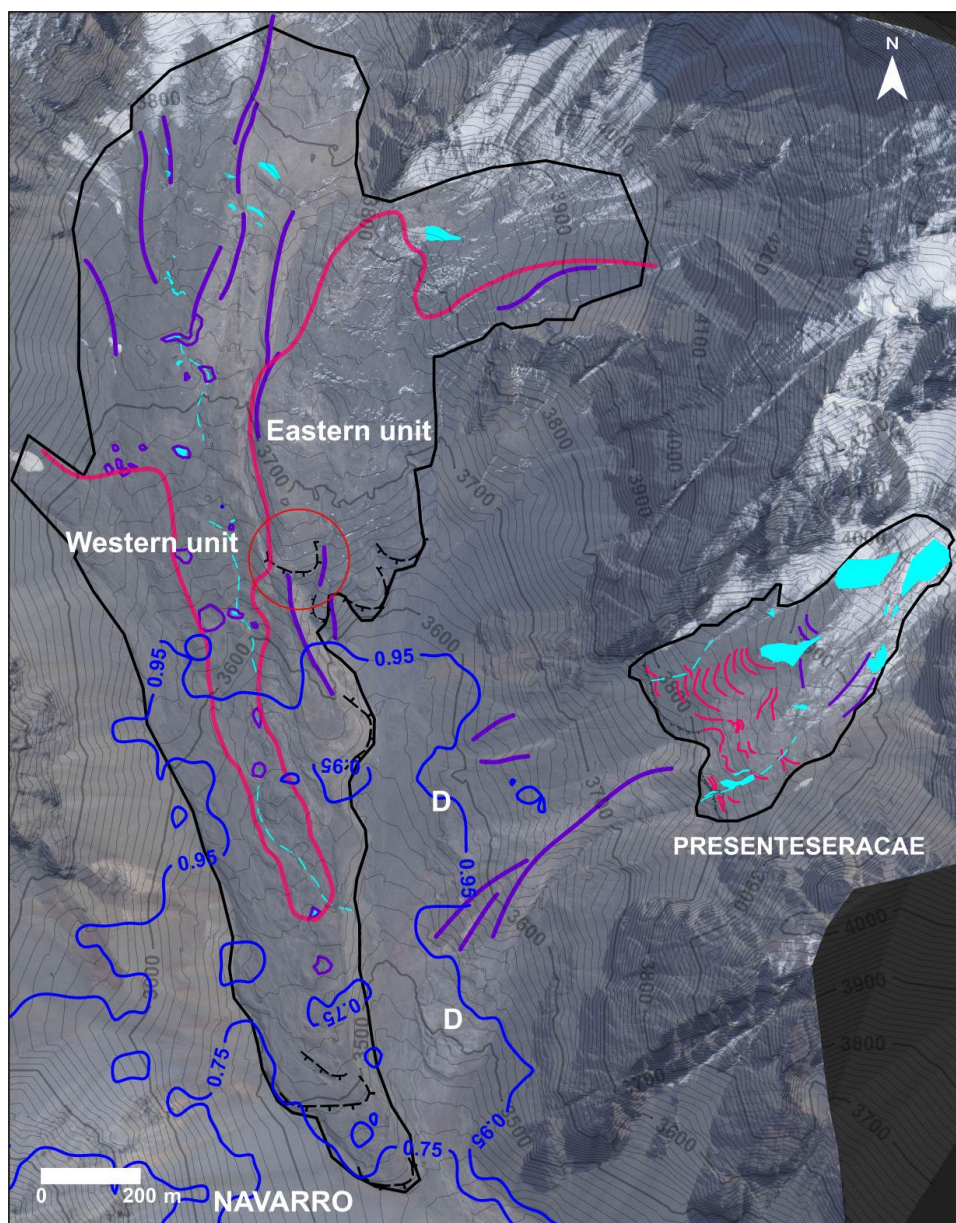
Figure 3. Map of the Navarro valley. See Fig. 2 for legend. The background of the map, as in Figs. 6
and 7, is the 2014 Geoeye image draped over the Geoeye DEM (see the Methods section). The red
circle indicates the location described in the text where morainic crests and rock glacier lobes are
superimposed. Note also the decayed (D) rock glacier lobes in the area between Navarro and
Presenteseracae.
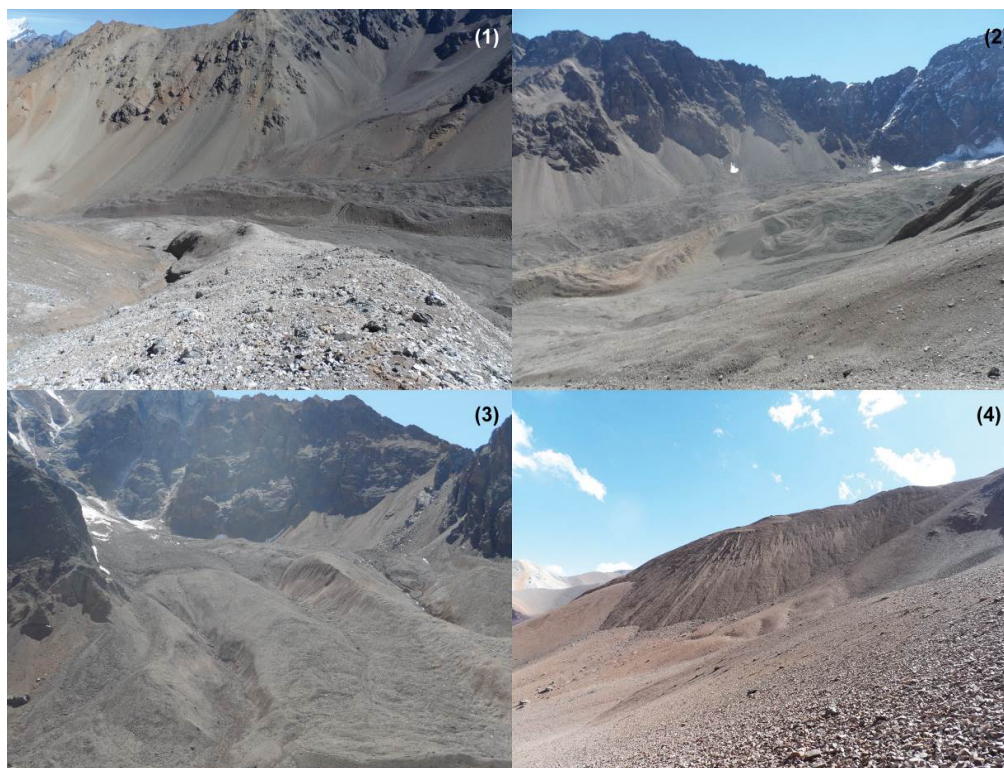
1

2 **Figure 4.** Photos of the lower (1) and upper part (2) of Navarro, seen from Presenteseracae,
3 Presenteseracae seen from Navarro (3), and the terminal part of Las Tetas (4) seen from its
4 northeastern surrounding area. Note the central depression and related thermokarst morphology on
5 Navarro.
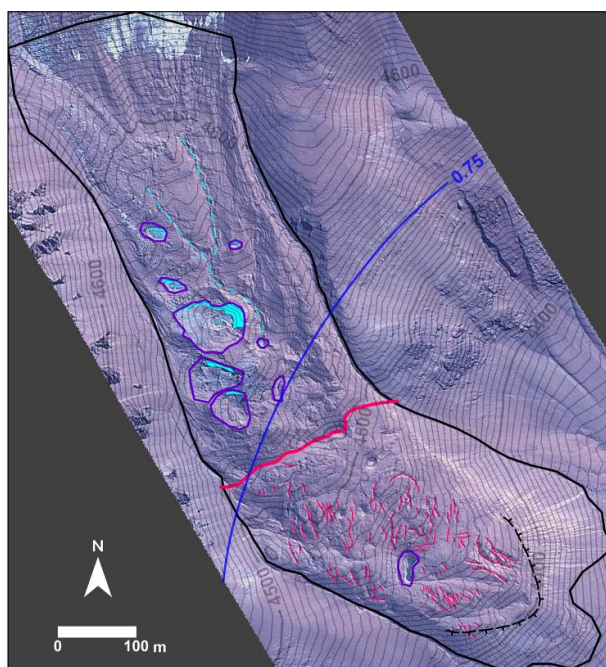
1

2　**Figure 5.** Map of the Las Tetas landform. See Fig. 2 for legend. The background of the map is the
3　2012 Geoeye image draped over the Geoeye DEM (see the Methods section).
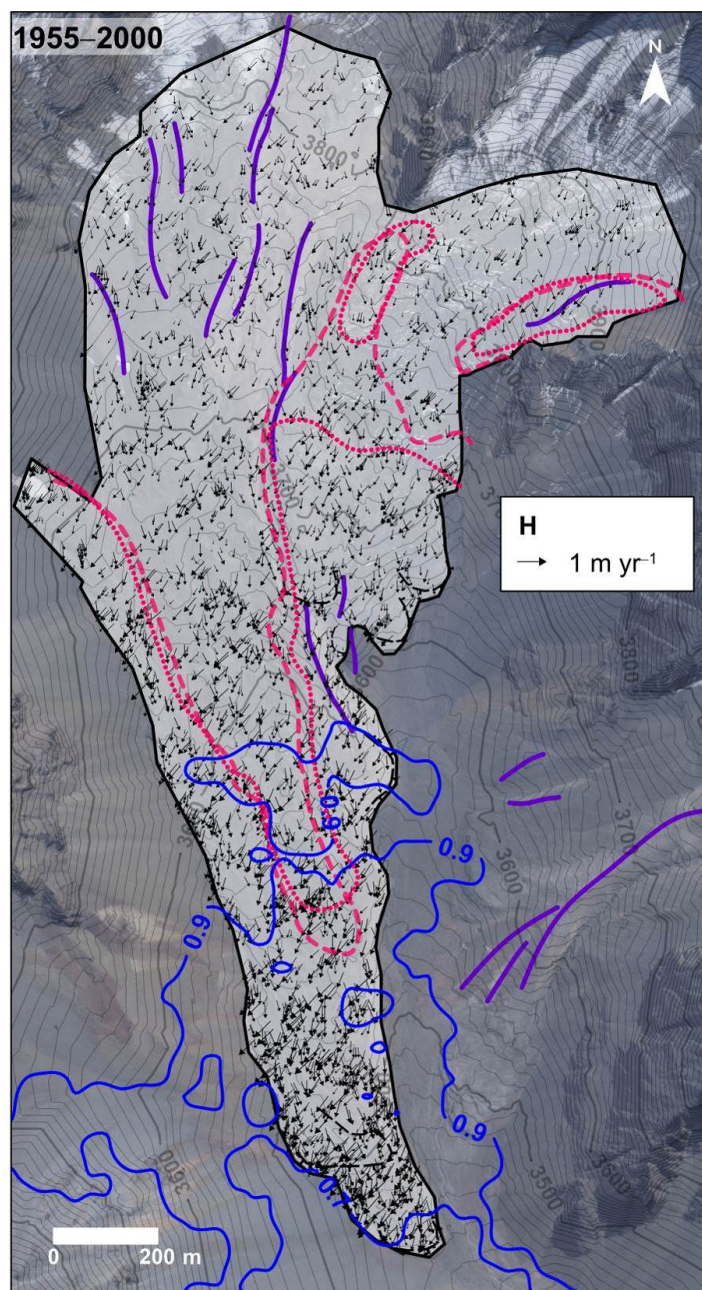
Figure 6. Horizontal (H) surface displacements of Navarro between 1955 and 2000. The boundary between the debris-covered and rock glacier morphologies is depicted with a dotted line in 1955 and a dashed line in 2000.
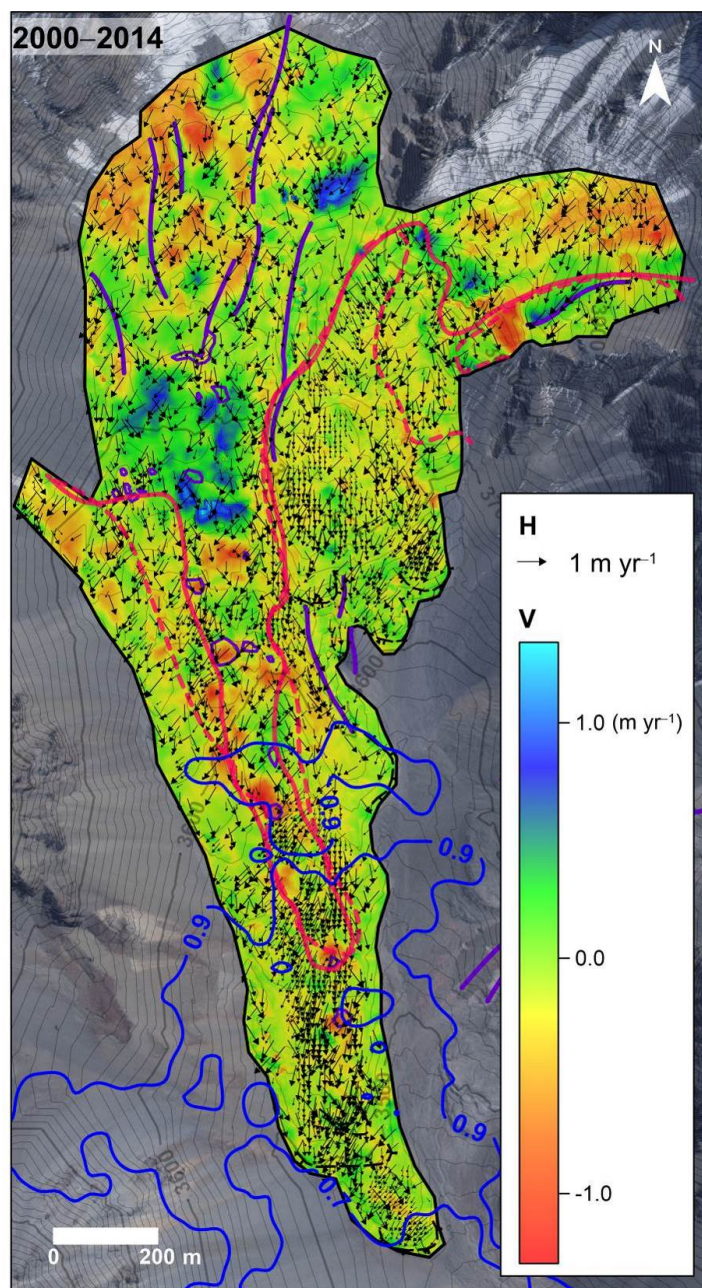
1

2 **Figure 7.** Horizontal (H) and vertical (V) displacements of Navarro between 2000 and 2014. The
3 boundary between debris-covered and rock glacier morphology is depicted with a dashed red line in
4 2000 and with a continuous red line in 2014.

1
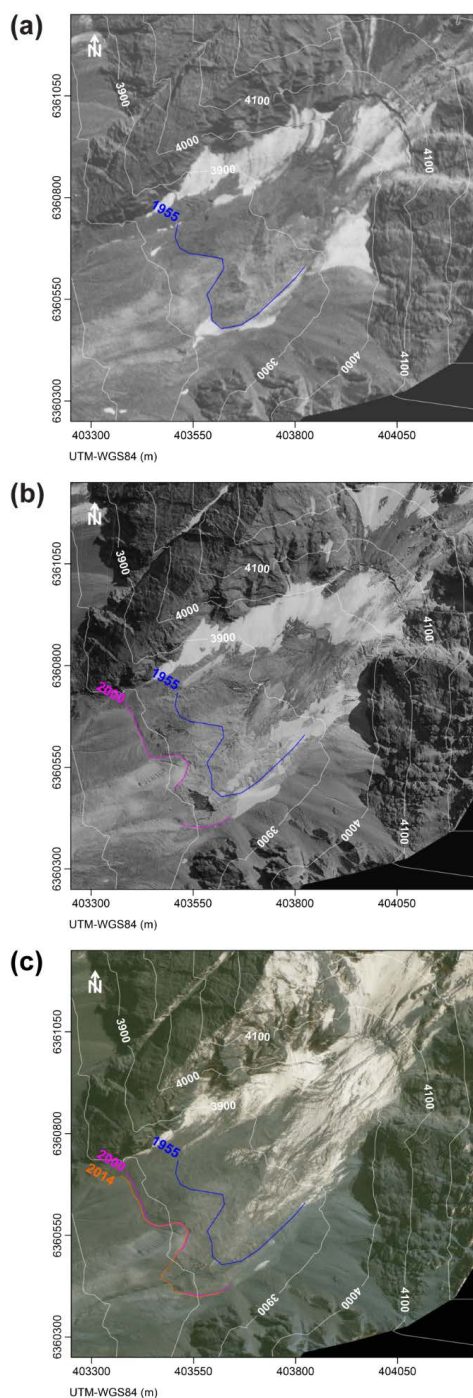
Figure 8. Advance and morphology changes of the Presenteseracae debris-covered glacier: 1955 (a),
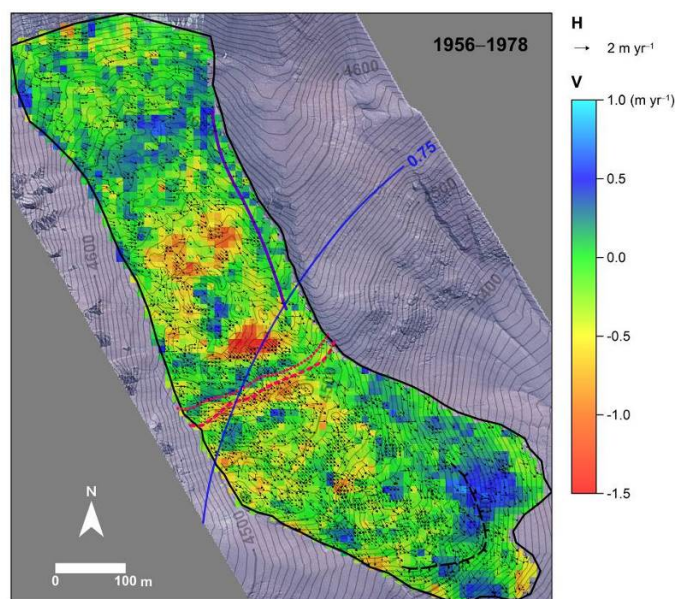2000 (b), and 2014 (c). The successive positions of the front base are delineated using colour lines.

1
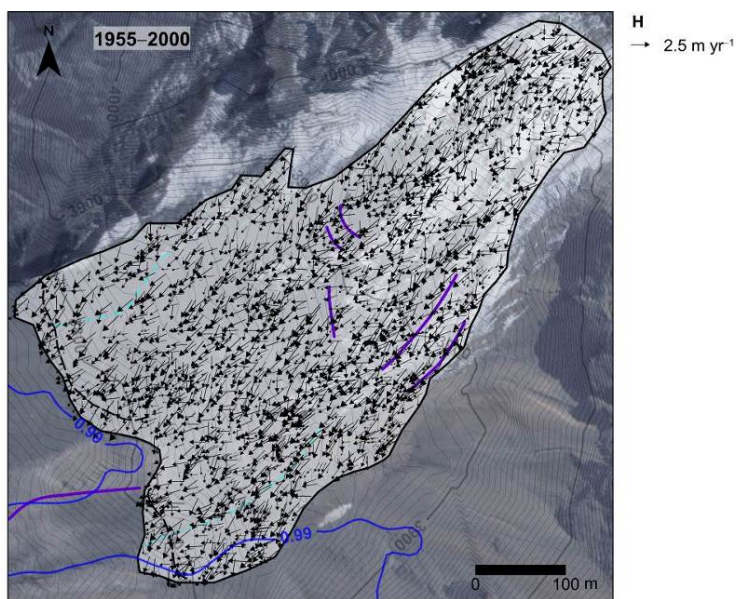
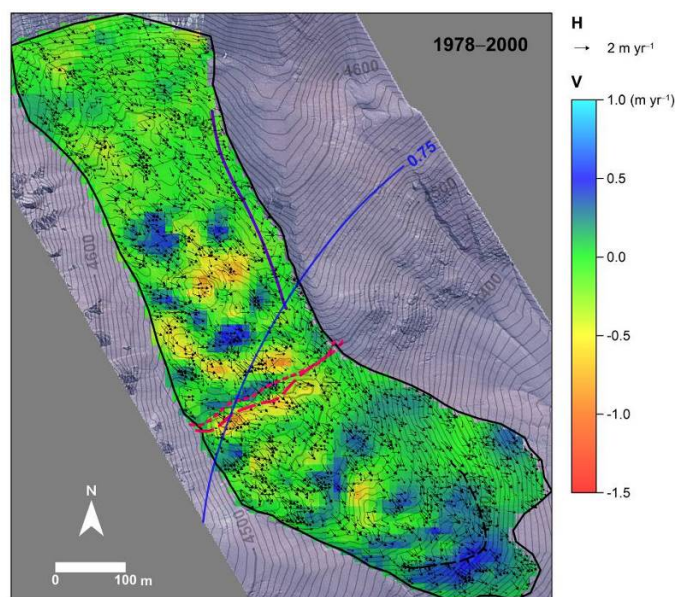2   **Figure 9.** Horizontal surface displacements (H) of Presenteseracae between 1955 and 2000.
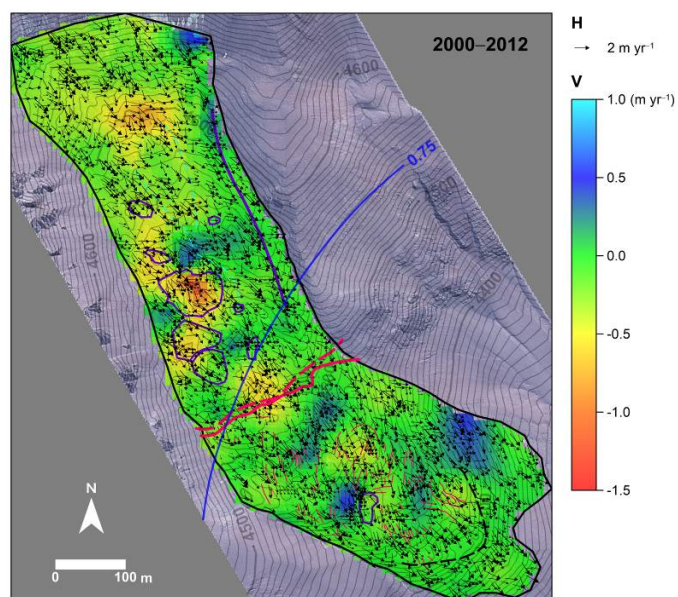
3

4
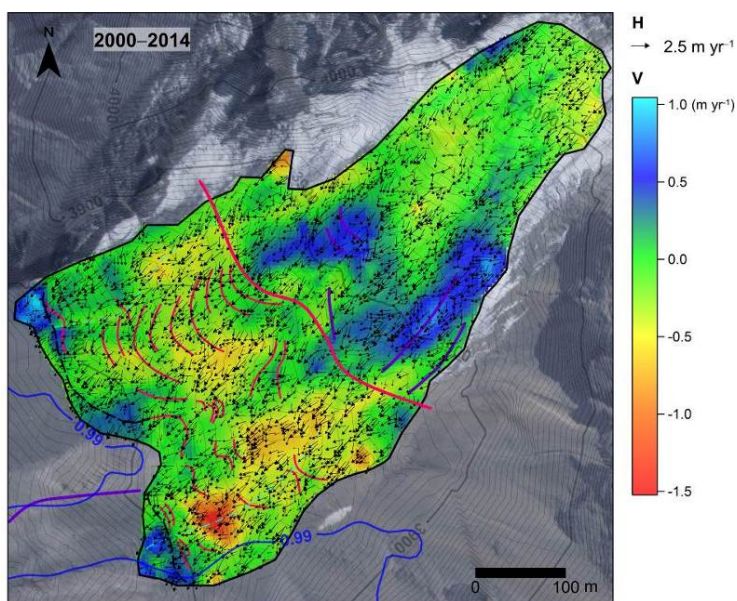
5   **Figure 10**. Horizontal (H) and vertical (V) surface displacements of Presenteseracae between 2000
6   and 2014.

1

Figure 11. Horizontal (H) and vertical (V) surface displacements of Las Tetas between 1956 and
1978. The boundary between debris-covered and rock glacier morphology is depicted with a dotted
line in 1956 and with a dashed line in 1978.

5

Figure 12. Horizontal (H) and vertical (V) surface displacements of Las Tetas between 1978 and
2000. The boundary between debris-covered and rock glacier morphology is depicted with a short
dashed line in 1978 and with a long dashed line in 2000.

1

Figure 13. Horizontal (H) and vertical (V) surface displacements of Las Tetas between 2000 and
2012. The boundary between debris-covered and rock glacier morphology is depicted with a dashed
line in 2000 and with a continuous line in 2012.